Engineering Notes

Controllability of Lorentz-Augmented Spacecraft Formations

Ludwik A. Sobiesiak* and Christopher J. Damaren†
University of Toronto, Toronto, Ontario M3H 5T6, Canada

DOI: 10.2514/1.G001148

Nomenclature

a	=	semimajor axis, m
$\boldsymbol{b}$	=	magnetic field vector, T
e	=	eccentricity
f	=	true anomaly, rad
h	=	specific angular momentum magnitude, m^2/s
i	=	inclination, rad
J_n	=	nth zonal harmonic coefficient
M	=	mean anomaly, rad
m	=	mass, kg
$\boldsymbol{m}$	=	magnetic dipole vector, $A \cdot m^2$
n	=	mean motion, rad/s
p	=	semilatus rectum, m
q	=	electrical charge, C
q_1	=	$e \cos \omega$
q_2	=	$e \sin \omega$
r	=	orbit radius magnitude, m
$\boldsymbol{r}$	=	position vector, m
$\boldsymbol{v}$	=	velocity vector, m/s
$\boldsymbol{W}$	=	controllability Gramian
$\boldsymbol{z}$	=	orbital element vector
ΔV	=	Delta-v magnitude, m/s
$\delta(t)$	=	Dirac Delta function
θ	=	true latitude, rad
λ	=	mean latitude, rad
μ	=	gravitational parameter, m^3/s^2
$\boldsymbol{\nu}$	=	Gramian eigenvector
$\boldsymbol{\Phi}$	=	state transition matrix
Ω	=	right ascension of ascending node, rad
$\boldsymbol{\omega}$	=	angular velocity vector, rad/s
ω	=	argument of periapsis, rad

Subscripts

c	=	chief
d	=	deputy
L	=	Lorentz force–related
r	=	reference quantity
$\oplus$	=	Earth-related quantity

Superscript

$\bar{(\cdot)}$	=	mean element quantity

Received 3 November 2014; revision received 14 July 2015; accepted for publication 22 July 2015; published online 17 September 2015.

*Ph.D. Graduate, Spacecraft Dynamics and Control Laboratory, University of Toronto Institute for Aerospace Studies, 4925 Dufferin Street.

†Professor, University of Toronto Institute for Aerospace Studies, 4925 Dufferin Street. Associate Fellow AIAA.

I. Introduction

THE geomagnetic Lorentz force represents a propellentless means of actuation for a spacecraft. The concept of Lorentz-force actuation is predicated on the spacecraft retaining and modulating an electrical charge so that the Earth's magnetic field acts on the spacecraft via the Lorentz force in a desirable fashion. Whether a spacecraft can generate and store sufficient electrical charge, and if the charge can be modulated by an energy-efficient means, is not yet clear. For a conventional spacecraft, it is prudent to mitigate charge accumulation via plasma contactors or particle beams. Although never used for such a purpose, such devices could also be used to accumulate additional charge. Studies into charge-carrying spacecraft suggest that existing technologies can be adapted to realize charge per unit mass, or specific charge, magnitudes between 10^{-6} and 10^{-3} C/kg [1]. Lorentz-augmented spacecraft architectures have been proposed in [2,3], however, to the authors' knowledge, no prototypes have been considered. In this Note, the means by which charge accumulation is achieved is not considered and it is assumed that the spacecraft has the required capability.

Although many different applications for Lorentz-force actuation have been studied, such as insertion in Jovian orbit [4] and Lorentz-augmented gravity assists [5], these applications typically require specific charge magnitudes that are orders of magnitude greater than those currently feasible. Conversely, spacecraft formation flight is a possible area of application for Lorentz-force actuation where the required specific charge magnitudes are closer to what is feasible. Past work has investigated in-plane Lorentz-augmented formation reconfiguration [6], formation stability [7], and three-dimensional reconfiguration [8]. Closed-form solutions to the relative-motion equations of spacecraft with a constant electrical charge were presented in [9]. Those works have considered the relative motion of the spacecraft in Cartesian coordinates using the Hill–Clohessy–Wiltshire or the Tschauner–Hempel equations to model the relative dynamics.

In this work, the relative dynamics are modeled using differential orbital elements, which are useful in providing additional insight into the Lorentz-augmented relative dynamics. The effects of the Lorentz force on the classical orbital elements have been fully described in [10] and also partially described and used in [11] to establish new J_2-invariant and ground-track-repeating orbits. Mean differential element formation control has been explored previously in [12,13], where it was identified that relative spacecraft dynamics are not completely controllable using solely the Lorentz force; optimal strategies combining the Lorentz force with either continuous or impulsive thruster actuation were proposed to fully control the relative dynamics.

The work in this Note characterizes the controllable and uncontrollable subspaces of the Lorentz-augmented mean differential orbital dynamics. The physical nature of the uncontrollable subspace is explained using the differential element representation of the relative dynamics and it is demonstrated that in some cases the relative dynamics are stabilizable in the sense of Lyapunov. A Lorentz-force only control strategy is designed to control the controllable subspace of the relative dynamics. Numerical simulations show it to be effective for both polar and equatorial orbits.

The remainder of the Note is structured as follows. Section II presents the linearized mean differential orbital elements dynamics

for the nonsingular orbital element set $\bar{z}=[\bar{a}\ \bar{i}\ \bar{\Omega}\ \bar{q}_1\ \bar{q}_2\ \bar{\lambda}]^T$; Sec. III introduces the geomagnetic Lorentz force, characterizes the controllable and uncontrollable subspaces of the Lorentz-augmented differential element system, and provides a physical explanation for the existence of the uncontrollable subspace. Section IV proposes the use of Kalman decomposition to separate the controllable and uncontrollable subspaces of the Lorentz-augmented orbital element system, despite it being a time-varying system; the use of Kalman decomposition is justified by demonstrating the uncontrollable subspace is time-invariant. A formation-keeping controller that employs only Lorentz-force actuation is designed using the controllable subspace of the decomposed system. The Note concludes with several numerical simulations demonstrating the efficacy of the Lorentz-force only controller for formation keeping in both equatorial and polar orbits.

II. Mean Differential Orbital Element Dynamics

The relative deputy spacecraft state with respect to the chief spacecraft is described by the differences between the actual mean orbital elements of the deputy and chief spacecraft

$$\delta\bar{z}(t) = \bar{z}_d(t) - \bar{z}_c(t) \tag{1}$$

where, in order to avoid numerical singularities that occur when eccentricity is zero, the nonsingular orbital element set, $\bar{z}=[\bar{a}\ \bar{i}\ \bar{\Omega}\ \bar{q}_1\ \bar{q}_2\ \bar{\lambda}]^T$, is used, where $\bar{q}_1=\bar{e}\cos\bar{\omega}$, $\bar{q}_2=\bar{e}\sin\bar{\omega}$, $\bar{\lambda}=\bar{M}+\bar{\omega}$. Because we are considering the J_2 zonal harmonic as the primary orbital perturbation affecting our formation, we employ mean elements, in the sense of Brouwer [14]. The use of mean elements results in only state errors caused by the secular growth in orbital elements due to J_2 to be corrected for, whereas the osculating variations in elements are ignored. The result is lower formation-keeping control effort.

For the nonsingular orbital element set, the vector of mean orbital element secular drift rates, $\boldsymbol{A}(\bar{z})$, is

$$\boldsymbol{A}(\bar{z}) = \begin{bmatrix} 0 \\ 0 \\ -\frac{3}{2}J_2\bar{n}\left(\frac{R_\oplus}{\bar{p}}\right)^2\cos\bar{i}, \\ -\bar{q}_2\dot{\bar{\omega}} \\ \bar{q}_1\dot{\bar{\omega}} \\ \dot{\bar{M}}+\dot{\bar{\omega}} \end{bmatrix} \tag{2}$$

where the argument of perigee and mean anomaly secular drift rates are

$$\dot{\bar{\omega}} = \frac{3}{4}J_2\bar{n}\left(\frac{R_\oplus}{\bar{p}}\right)^2(5\cos^2\bar{i}-1) \tag{3}$$

$$\dot{\bar{M}} = \bar{n}+\frac{3}{4}J_2\bar{n}\,\bar{\eta}\left(\frac{R_\oplus}{\bar{p}}\right)^2(3\cos^2\bar{i}-1) \tag{4}$$

The effect of an applied control effort or additional perturbation can be related to changes in the orbital elements using Gauss's variational equations, which are

$$\boldsymbol{B}(z) = \begin{bmatrix} \frac{2a^2e\sin f}{h} & \frac{2a^2p}{rh} & 0 \\ 0 & 0 & \frac{r\cos\theta}{h} \\ 0 & 0 & \frac{r\sin\theta}{h\sin i} \\ \frac{p\sin\theta}{h} & \frac{(p+r)\cos\theta+re\cos\omega}{h} & \frac{re}{h}\frac{\sin\omega\sin\theta}{\tan i} \\ -\frac{p\cos\theta}{h} & \frac{(p+r)\sin\theta+re\sin\omega}{h} & -\frac{re}{h}\frac{\cos\omega\sin\theta}{\tan i} \\ -\frac{pe\cos f}{h(1+\eta)}-\frac{2r\eta}{h} & \frac{(p+r)}{(1+\eta)}\frac{e\sin f}{h} & -\frac{r\sin\theta}{h\tan i} \end{bmatrix} \tag{5}$$

and where $\eta=\sqrt{1-q_1^2-q_2^2}$, $p=a\eta^2$, and $h=\sqrt{\mu p}$. It is understood that $\boldsymbol{B}$ will vary with time, due to the dependence on true anomaly f. Together, Eqs. (2) and (5) describe the mean nonsingular element dynamics

$$\dot{\bar{z}} = \boldsymbol{A}(\bar{z}) + \frac{\partial\epsilon(\bar{z})^T}{\partial z}\boldsymbol{B}(z)\boldsymbol{u}(t) \tag{6}$$

where $\boldsymbol{u}(t)$ is the applied acceleration vector, expressed in the local vertical/local horizontal (LVLH) frame, illustrated in Fig. 1. The origin of the LVLH frame is at the position of the spacecraft; the one-axis, $\hat{\underset{\rightarrow r}{1}}$, is in the outward direction of the spacecraft's position axis; the three-axis, $\hat{\underset{\rightarrow h}{1}}$, is parallel with the spacecraft's orbit's angular momentum vector; and the two-axis, $\hat{\underset{\rightarrow\theta}{1}}$, completes the right-hand rule. The relative position of the deputy spacecraft with respect to the chief is typically described in the LVLH frame positioned at the chief spacecraft. The expression $\partial\epsilon(\bar{z})/\partial z$ is the partial derivative of the transformation function from osculating to mean elements. A first-order analytical expression of it appears in [15]; however, for control design purposes it can approximated by identity [16].

A reference vector of differential elements, $\delta\bar{z}_r$, describes the desired relative trajectory of the deputy spacecraft. We are interested in regulating the error in the deputy's differential orbital elements

$$\boldsymbol{x}(t) = \bar{z}_d(t) - \bar{z}_r \quad = \delta\bar{z} - \delta\bar{z}_r \tag{7}$$

The error dynamics are

$$\dot{\boldsymbol{x}}(t) = \dot{\bar{z}}_d - \dot{\bar{z}}_r \tag{8}$$

Linearizing the dynamics about the reference orbital elements, $\bar{z}_r$ yields

$$\dot{\boldsymbol{x}}(t) = \dot{\bar{z}}_r + \left.\frac{\partial\boldsymbol{A}(\bar{z})}{\partial\bar{z}}\right|_{\bar{z}=\bar{z}_r}\boldsymbol{x}(t) + \left(\boldsymbol{B}(\bar{z}_r) + \left.\frac{\partial\boldsymbol{B}}{\partial\bar{z}}\right|_{\bar{z}=\bar{z}_r}\boldsymbol{x}(t)\right)\boldsymbol{u}(t) - \dot{\bar{z}}_r \tag{9}$$

$$= \tilde{\boldsymbol{A}}(\bar{z}_r)\boldsymbol{x}(t) + \boldsymbol{B}(\bar{z}_r)\boldsymbol{u}(t) \tag{10}$$

where for the nonsingular elements

$$\tilde{\mathbf{A}}(\bar{z}_r) = \left[\begin{array}{cccc|c} & & \mathbf{0}_{2\times4} & & \mathbf{0}_{2\times2} \\ \hline \frac{\partial\dot{\bar{\Omega}}}{\partial\bar{a}} & \frac{\partial\dot{\bar{\Omega}}}{\partial\bar{i}} & \frac{\partial\dot{\bar{\Omega}}}{\partial\bar{q}_1} & \frac{\partial\dot{\bar{\Omega}}}{\partial\bar{q}_2} & \\ \frac{\partial\dot{\bar{q}}_1}{\partial\bar{a}} & \frac{\partial\dot{\bar{q}}_1}{\partial\bar{i}} & \frac{\partial\dot{\bar{q}}_1}{\partial\bar{q}_1} & \frac{\partial\dot{\bar{q}}_1}{\partial\bar{q}_2}-\dot{\bar{\omega}} & \mathbf{0}_{4\times2} \\ \frac{\partial\dot{\bar{q}}_2}{\partial\bar{a}} & \frac{\partial\dot{\bar{q}}_2}{\partial\bar{i}} & \frac{\partial\dot{\bar{q}}_2}{\partial\bar{q}_1}+\dot{\bar{\omega}} & \frac{\partial\dot{\bar{q}}_2}{\partial\bar{q}_2} & \\ \frac{\partial\dot{\bar{\lambda}}}{\partial\bar{a}} & \frac{\partial\dot{\bar{\lambda}}}{\partial\bar{i}} & \frac{\partial\dot{\bar{\lambda}}}{\partial\bar{q}_1} & \frac{\partial\dot{\bar{\lambda}}}{\partial\bar{q}_2} & \end{array}\right] \tag{11}$$

Per [17], $\partial\boldsymbol{B}/\partial\bar{z}$ can be neglected for spacecraft relative separations and velocities of approximately 25 km and 40 m/s when considering formations in low Earth orbit (LEO).

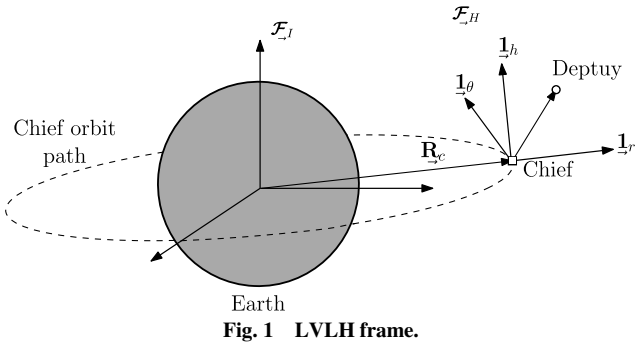

Fig. 1 LVLH frame.

III. Controllability of the Lorentz-Augmented System

The Lorentz acceleration vector acting on charged spacecraft, expressed in an Earth-fixed inertial frame, is

$$\boldsymbol{f}_L = \frac{q(t)}{m}\boldsymbol{v}_{\text{rel}}(t) \times \boldsymbol{b}_{\oplus}(t, \boldsymbol{z}) \tag{12}$$

where $\boldsymbol{b}_{\oplus}(t, \boldsymbol{z})$ is the geomagnetic field vector at the spacecraft's location and $q(t)/m$ is the ratio of charge to mass on the spacecraft known as the specific charge. The spacecraft's velocity relative to the geomagnetic field is

$$\boldsymbol{v}_{\text{rel}}(t) = \boldsymbol{v}(t) - \boldsymbol{\omega}_{\oplus} \times \boldsymbol{r}(t) \tag{13}$$

where $\boldsymbol{r}$ and $\boldsymbol{v}$ are the spacecraft's inertial position and velocity vectors and $\boldsymbol{\omega}_{\oplus}$ is the Earth's angular velocity.

The Lorentz-augmented differential element error dynamics are

$$\dot{\boldsymbol{x}} = \tilde{\boldsymbol{A}}(\bar{\boldsymbol{z}}_r)\boldsymbol{x}(t) + \tilde{\boldsymbol{B}}(\bar{\boldsymbol{z}}_r)u(t) \tag{14}$$

where the new input matrix is

$$\tilde{\boldsymbol{B}}(\bar{\boldsymbol{z}}_r) = \boldsymbol{B}(\bar{\boldsymbol{z}}_r)(\boldsymbol{v}_{\text{rel}}(t) \times \boldsymbol{b}_{\oplus}(t, \bar{\boldsymbol{z}}_r)) \tag{15}$$

and the sole control input is the specific charge $u(t) = (q(t)/m)$. From previous work [13], it is known that the system described by Eq. (14) is not fully controllable. For a given reference orbit, calculating the controllability Gramian and determining its eigenvalues reveals that the Gramian poses one eigenvalue equal to zero and is singular. This result was shown to hold across all inclinations and for all semimajor axes in LEO.

This result is examined in more detail in this section. Specifically, the nature of the uncontrollable mode is sought. The controllability Gramian is given by

$$\boldsymbol{W}(t_1, t_0) = \int_{t_0}^{t_1} \boldsymbol{\Phi}(t_1, \tau)\boldsymbol{B}(\tau)\boldsymbol{B}^T(\tau)\boldsymbol{\Phi}^T(t_1, \tau)\,\mathrm{d}\tau \tag{16}$$

where $\boldsymbol{\Phi}(t, \tau)$ is the state transition matrix of the linear system and $\boldsymbol{B}(t)$ is the system's input matrix. The controllability matrix was also calculated in [18] for different applications. For a singular Gramian, the eigenvector of the Gramian associated with the zero eigenvalue, $\boldsymbol{\nu}_0 = [\nu_{0_a} \quad \nu_{0_i} \quad \nu_{0_\Omega} \quad \nu_{0_{q1}} \quad \nu_{0_{q2}} \quad \nu_{0_i}]^T$, describes the uncontrollable subspace of the system. The uncontrollable mode is determined for controllability Gramians calculated for reference orbits ranging in semimajor axis and inclination of $a = 6639.2{-}12,000$ km and $i = 0{-}90$ deg, respectively, and a constant eccentricity of $e = 0.001$. The time interval over which the Gramian is calculated is the synodic period of the spacecraft with respect to the geomagnetic field, i.e., the time it takes for the spacecraft to reach the same point in the Earth's magnetic field. As has been previously noted [9,13], this is the natural period of the magnetic field variations seen by the spacecraft. Figure 2 illustrates the dominant components of $\boldsymbol{\nu}_0$, namely ν_{0_a} and ν_{0_i}. The remaining four components are consistently of order $\mathcal{O}(10^{-3})$ or smaller, and are not shown.

The main component of the uncontrollable mode, for all the considered orbits, is the component associated with differential semimajor axis, ν_{0_a}. For near-equatorial orbits, Fig. 2a shows that ν_{0_a} is close to 1, regardless of inclination.

For near-equatorial orbits with relatively small semimajor axes, the mean differential semimajor axis is effectively the uncontrollable state in the Lorentz-augmented system. The work of Tsujii et al. [8] corresponds with this result. In [8], analysis of Lorentz-augmented Hill–Clohessy–Wiltshire equations — linear relative-motion equations that are valid for circular orbits — for the equatorial orbit case revealed that the in-plane uncontrollable state is $x_4 = 2x + \mathrm{d}y/\mathrm{d}f$, where x and y are the radial and along-track position components in the LVLH frame. It is shown in [16], for $e = 0$, that this state is equivalent to δa and is the expression that must be set to zero to ensure bounded relative motion between two spacecraft in Keplerian orbits. The physical reason for the lack of controllability of differential semimajor axis can be seen by considering Gauss's variational equations for the semimajor axis

$$\frac{\mathrm{d}a}{\mathrm{d}t} = \begin{bmatrix} \frac{2a^2 e \sin f}{h} & \frac{2a^2 p}{rh} & 0 \end{bmatrix} \begin{bmatrix} u_r(t) \\ u_\theta(t) \\ u_h(t) \end{bmatrix} \tag{17}$$

In near-circular orbits, as would be the case for a formation in low Earth orbit (LEO), the radial component of Eq. (17) vanishes, leaving only the along-track component. The Lorentz-force component in the along-track direction, however, is very small because it acts in a direction that is perpendicular to both the local geomagnetic field vector and the spacecraft's velocity relative to geomagnetic field. For LEOs, the term $-\boldsymbol{\omega}_{\oplus} \times \boldsymbol{r}(t)$ is small, so $\boldsymbol{v}_{\text{rel}}(t) \approx \boldsymbol{v}(t)$. Thus, the Lorentz force is nearly perpendicular to the spacecraft's velocity and, likewise, to the along-track direction, resulting in the differential semimajor axis being pointwise underactuated. However, it should not be discounted that the term $-\boldsymbol{\omega}_{\oplus} \times \boldsymbol{r}(t)$ may have long-term effects.

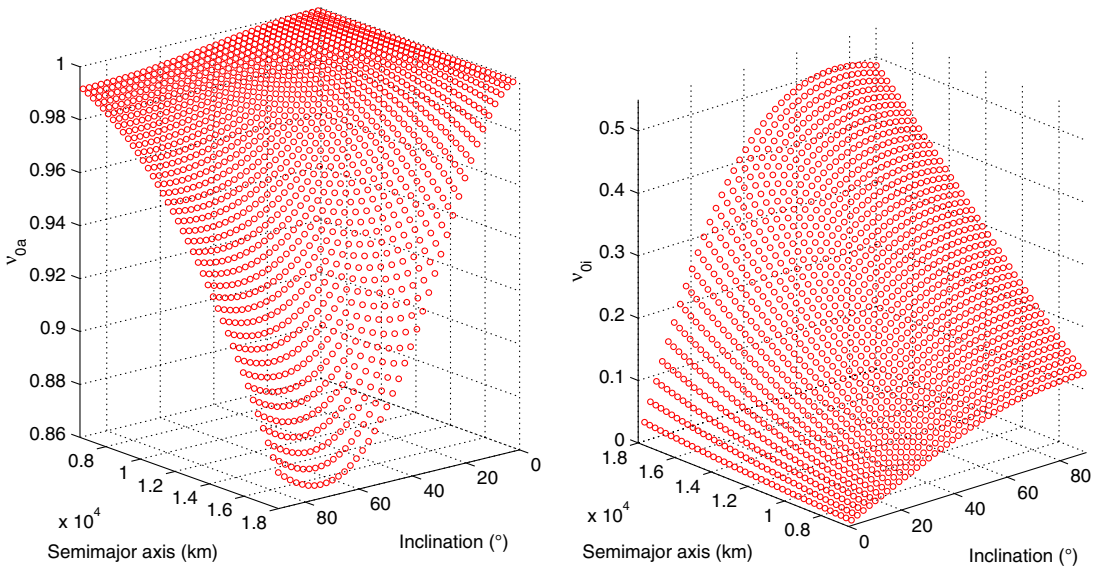

a) $\boldsymbol{\nu}_{0_a}$ component **b) $\boldsymbol{\nu}_{0_i}$ component**

Fig. 2 Dominant components of the uncontrollable mode, $\boldsymbol{\nu}_0$, of the Lorentz-augmented mean differential element system.

As semimajor axis and inclination increase, the uncontrollable state becomes a linear combination of differential semimajor axis and differential inclination. The component associated with differential inclination, ν_{0_i}, becomes significant with nonzero inclination and can be of the same order of magnitude as ν_{0_a}, although ν_{0_a} remains the dominant component. In particular, for nonzero inclinations but small semimajor axes, ν_{0_i} continues to be small and the previous discussion regarding the physical reason for $\delta\bar{a}$ being uncontrollable continues to hold. For reference orbits with a large semimajor axis, the approximation $\boldsymbol{v}_{\text{rel}}(t) \approx \boldsymbol{v}(t)$ is a poor one, because the $-\boldsymbol{\omega}_{\oplus} \times \boldsymbol{r}(t)$ term is too large to neglect. Consequently, the uncontrollable mode is no longer just the differential semimajor axis. Figure 2b shows ν_{0_i} to be significant at large semimajor axis, particularly for inclinations greater than 60 deg. Lastly, the behavior of the eigenvectors of the controllability Gramian is examined as the interval over which the Gramian is calculated is varied.

IV. Formation Control

Previous work [12,13] on the subject of formation keeping using the Lorentz force has focused on supplementing Lorentz-force actuation with thruster actuation in order to achieve controllability of the system. Using impulsive thruster actuation [13] was shown to be particularly effective in maintaining the desired formation while also minimizing the required amount of the thruster control effort.

A. Kalman Decomposition of the Lorentz-Augmented System

Performing Kalman decomposition on the linear, time-invariant (LTI) system is a classical method for decomposing a system into its controllable and uncontrollable modes. Consider the matrix $\boldsymbol{T} = [\boldsymbol{T}_c \quad \boldsymbol{T}_u]$, where the columns of $\boldsymbol{T}_c$ span the controllable subspace of the system and the columns of $\boldsymbol{T}_u$ span the system's uncontrollable subspace and, in doing so, complement $\boldsymbol{T}_c$, such that $\boldsymbol{T}$ is invertible. The matrix $\boldsymbol{T}$ can be used to perform a similarity transformation on a LTI system with state and input matrices $(\boldsymbol{A}, \boldsymbol{B})$, such that

$$\hat{\boldsymbol{A}} = \boldsymbol{T}^{-1}\boldsymbol{A}\boldsymbol{T} = \begin{bmatrix} \hat{\boldsymbol{A}}_c & \hat{\boldsymbol{A}}_{cu} \\ 0 & \hat{\boldsymbol{A}}_u \end{bmatrix}, \qquad \hat{\boldsymbol{B}} = \boldsymbol{T}^{-1}\boldsymbol{B} = \begin{bmatrix} \hat{\boldsymbol{B}}_c \\ 0 \end{bmatrix}$$

The transformation matrix $\boldsymbol{T}$ can be constructed by using the eigenvectors of the system's controllability Gramian for the columns of $\boldsymbol{T}$. When doing so, $\boldsymbol{T}^{-1} = \boldsymbol{T}^T$, because the eigenvectors are orthogonal.

The Lorentz-augmented mean differential element system is not time-invariant: it possesses a time-varying input matrix, $\boldsymbol{B}(\bar{z}_r)$. Gauss's variational equations and the local geomagnetic field vector vary with the spacecraft's true anomaly. Its state matrix, $\tilde{\boldsymbol{A}}(\bar{z}_r)$, however, is time-invariant: the differential J_2 drift rates are functions of only $\bar{a}$, $\bar{e}$, and $\bar{i}$, which do not undergo secular change. If the controllable and uncontrollable subspaces of the Lorentz-augmented system are invariant with time, i.e., the columns of $\boldsymbol{T}$ are time-invariant for the Lorentz-augmented system, then the Lorentz-augmented system can be decomposed into controllable and uncontrollable spaces. To determine whether $\boldsymbol{T}$ is time-invariant for the Lorentz-augmented differential element system, the system's controllability Gramian, $\boldsymbol{W}(t_1, t_0)$, is calculated for different control intervals, $\Delta t = t_1 - t_0$, and the behavior of its eigenvectors is examined.

1. Formations in Polar Orbits

The component magnitudes of the six eigenvectors of the controllability Gramian and how they change with the interval over which the Gramian was calculated, Δt, are plotted in Fig. 3 for the case of a circular, polar reference orbit with a semimajor axis of $\bar{a} = 6945.033$ km. The eigenvector $\boldsymbol{\nu}_0$ is the uncontrollable mode.

For this polar orbit example, the uncontrollable mode, seen in Fig. 3a, is effectively time-invariant. The two dominant components, ν_{0_a} ν_{0_i}, are approximately constant for $t_1 < 300$. Because $\boldsymbol{\nu}_0$ is approximately time-invariant then so is the subspace it spans. Although Figs. 3b and 3c clearly show that components of other eigenvectors do vary significantly with the Gramian interval, this variation is not a problem. Because the uncontrollable subspace is invariant with respect to Δt, then so is its complementary subspace, the controllable subspace. Consequently, so long as the uncontrollable mode is Δt-invariant, it does not matter if the eigenvectors describing the controllable subspace vary with Δt, because the subspace itself is not changing.

2. Formations in Near-Equatorial Orbits

Figure 4 plots the evolution of eigenvector component magnitudes versus the Gramian interval Δt for the case of a circular, near-equatorial ($\bar{i} = 1$ deg) reference orbit with a semimajor axis of $\bar{a} = 6945.033$ km. As in the polar orbit example, $\boldsymbol{\nu}_0$ is the uncontrollable mode. For a near-equatorial reference orbit, four out of the six eigenvectors, $\boldsymbol{\nu}_0, \boldsymbol{\nu}_3, \boldsymbol{\nu}_4$, and $\boldsymbol{\nu}_5$, are effectively invariant with respect to Δt. As in the polar case, this includes the uncontrollable mode. Each of the aforementioned eigenvectors has either one or two dominant components that do not vary with Δt, and although the remaining components do vary with Δt, their magnitudes are sufficiently small to be considered negligible. The eigenvectors $\boldsymbol{\nu}_1$ and $\boldsymbol{\nu}_2$ do vary with Δt. By the argument of the previous section, because the uncontrollable mode, and thus the uncontrollable subspace, is Δt-invariant, then so is the controllable subspace.

Therefore, for both the polar and equatorial reference orbit, it is possible to perform Kalman decomposition on the Lorentz-augmented differential element system. For other inclinations, a similar analysis to the one performed previously is required.

B. Controller Formulation

The design of a feedback controller for the decomposed Lorentz-augmented differential element system is now considered. The decomposed mean differential element error system has the form

$$\dot{\hat{\boldsymbol{x}}}_c(t) = \hat{\boldsymbol{A}}_c\hat{\boldsymbol{x}}_c(t) + \hat{\boldsymbol{B}}_c(t)u(t) \tag{18}$$

where $\hat{\boldsymbol{A}}_c = \boldsymbol{T}_c^T\tilde{\boldsymbol{A}}(\bar{z}_r)\boldsymbol{T}_c$, $\hat{\boldsymbol{B}}_c(t) = \boldsymbol{T}^T\tilde{\boldsymbol{B}}(\bar{z}_r)$, $\hat{\boldsymbol{x}}_c(t) = \boldsymbol{T}_c^T\boldsymbol{x}(t)$, and $u(t) = q(t)/m$. We find that the uncontrollable mode is stabilizable in the sense of Lyapunov, i.e., that its eigenvalue lies on the imaginary axis. Therefore, although it is not stable in an input–output sense, if the mode is not excited by an initial error, it will not impact the formation. It follows then that a linear quadratic regulator (LQR)-style feedback control law of the form

$$u(t) = -R^{-1}\hat{\boldsymbol{B}}_c^T(t)\boldsymbol{P}(t)\hat{\boldsymbol{x}}_c(t) \tag{19}$$

can be chosen for control, where only the controllable states are used for feedback. Rather than solving the time-varying matrix Riccati equation for a history of $\boldsymbol{P}(t)$, the constant, asymptotic limit of the time-varying Riccati equation, $\boldsymbol{P}_{\text{ss}}$, is calculated, as proposed by Psiaki [19]. The asymptotic gain $\boldsymbol{P}_{\text{ss}}$ is obtained by solving the matrix algebraic Riccati equation

$$0 = \boldsymbol{P}_{\text{ss}}\hat{\boldsymbol{A}}_c + \hat{\boldsymbol{A}}_c^T\boldsymbol{P}_{\text{ss}} - \boldsymbol{P}_{\text{ss}}\hat{\boldsymbol{B}}_{\text{ss}}\hat{\boldsymbol{B}}_{\text{ss}}^T\boldsymbol{P}_{\text{ss}} + \boldsymbol{Q} \tag{20}$$

where $\hat{\boldsymbol{B}}_{\text{ss}}$ is obtained by performing the square-root factorization

$$\hat{\boldsymbol{B}}_{\text{ss}}\hat{\boldsymbol{B}}_{\text{ss}}^T = \frac{1}{t_f - t_0}\int_{t_0}^{t_f} \hat{\boldsymbol{B}}_c(\tau)R^{-1}\hat{\boldsymbol{B}}_c^T(\tau)\,\mathrm{d}\tau \tag{21}$$

Although the Lorentz-augmented mean differential element system violates Psiaki's stipulation that $\hat{\boldsymbol{A}}_c$ have no eigenvalues in the right-half plane, we find that the method still works well in simulation.

V. Numerical Examples

The proposed control strategy is validated using numerical integration of the nonlinear equations of motion of the chief and deputy spacecraft. The tilted dipole model [20] is used to model the geomagnetic field and

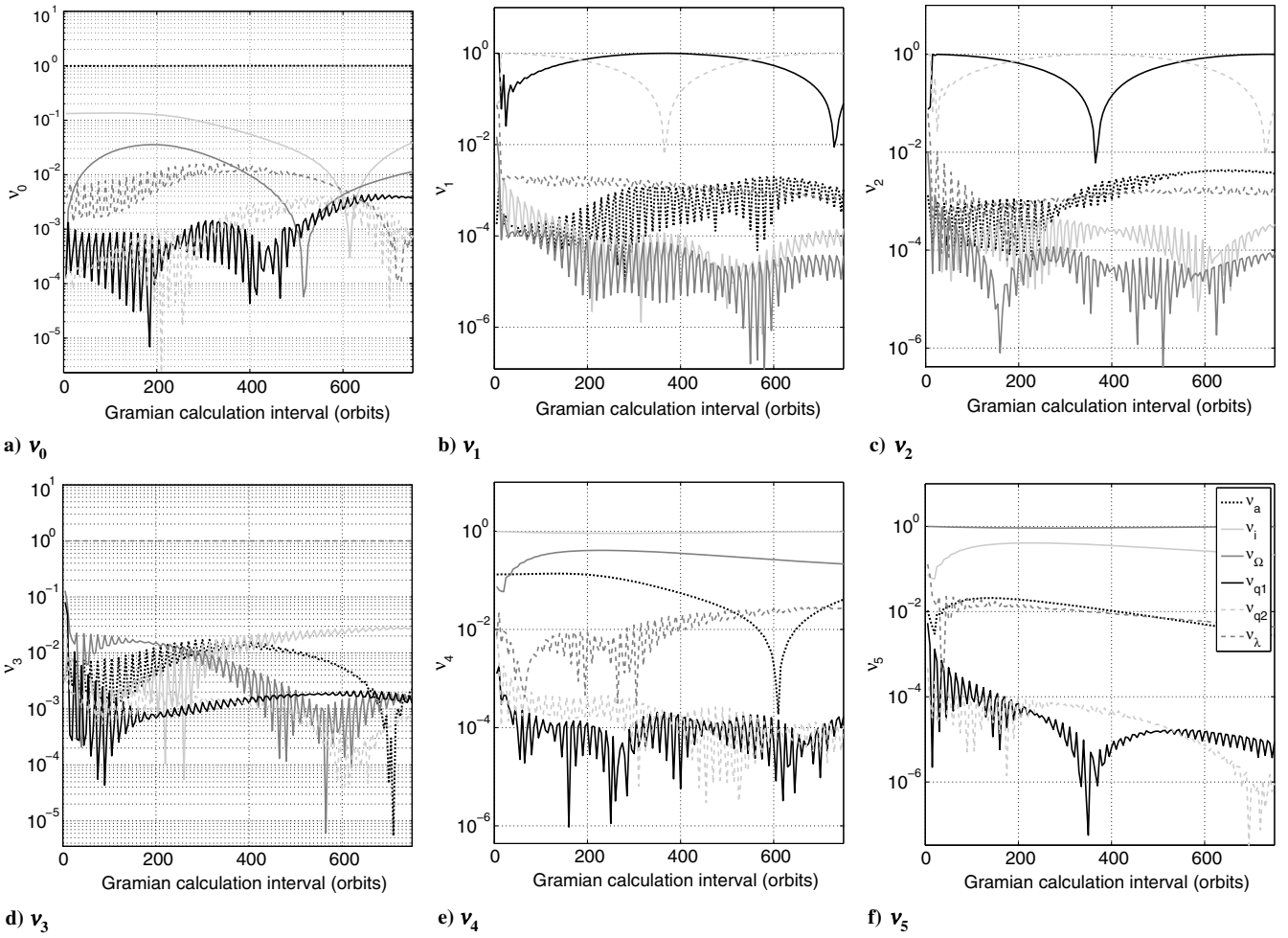

Fig. 3 Component magnitudes of the eigenvectors ν_0–ν_5 of the controllability Gramian for the Lorentz-augmented differential element system, for a polar, LEO.

the only orbital perturbation is the J_2 zonal harmonic. The formation keeping of a 1 km project circular orbit (PCO) formation, with an initial phase angle of 0 deg, is considered in both polar and equatorial orbits. The mean orbital elements of the chief spacecraft and the reference differential elements for the two cases are presented in Table 1. The deputy spacecraft is initialized to the correct formation.

For both reference orbits, we confirm that the transformed input matrix has the desired form $\hat{\boldsymbol{B}}(t) = [\hat{\boldsymbol{B}}_c{}^T(t)\ 0]^T$. Figure 5 plots the magnitudes of the components of $\hat{\boldsymbol{B}}(t)$, with $\hat{B}_0(t)$ denoting the component corresponding to the uncontrollable mode. For the equatorial orbit, Fig. 5a shows that $\hat{B}_0(t)$ is consistently several orders of magnitude smaller than the next smallest component of $\hat{\boldsymbol{B}}(t)$. For the polar case, Fig. 5b shows that $\hat{B}_0(t)$ is, on average, the smallest component of the transformed input matrix by at least an order of magnitude; however, there are brief instants when other components of $\hat{\boldsymbol{B}}(t)$ are momentarily smaller than $\hat{B}_0(t)$.

For the calculations of the controllability Gramian and the averaged input matrix $\hat{\boldsymbol{B}}_{\text{ss}}$, a time interval of 15 orbits was used, which corresponds to the synodic period of the spacecraft with respect to the geomagnetic field. For the equatorial reference orbit, the LQR design weights are

$$\boldsymbol{Q} = 5 \times 10^7 \cdot \mathbf{1}, \qquad R = 10^3$$

and for the polar reference orbit

$$\boldsymbol{Q} = 9.6 \times 10^6 \cdot \mathbf{1}, \qquad R = 3.5 \times 10^3$$

The asymptotic LQR controllers designed for the controllable portion of the Lorentz-augmented mean differential element system are effective at maintaining the desired 1 km formation and keeping the differential element errors, and thus, the relative position errors, bounded. Because they provide a more intuitive sense of how well the controllers perform, the relative position errors in the LVLH frame are presented in Fig. 6 for the two test cases, rather than the differential element errors. For the formation in an equatorial orbit, the norm of the relative position error has a maximum amplitude of approximately 35 m, with the largest error being in the along-track direction and the smallest error is in the out-of-plane direction. For the formation in polar orbit, the norm of the position error is smaller than in the equatorial case, with maximum amplitude of approximately 18 m. Converse to the equatorial case, the largest position errors occur in the out-of-plane direction, whereas the least error is in the radial position. For both cases, the specific charge required for formation keeping is on the order of 10^{-4} C/kg. For both cases, the error is periodic with a period of 15 orbits, which is equal to the synodic period of the spacecraft.

Thus, formation maintenance is possible using the Lorentz force alone, assuming the spacecraft begins in its desired formation. The formation error achieved is coarse, but remains bounded. This motivates the use of combined thruster/Lorentz-force controller strategies [12,13], which achieve position errors on the order of meters, rather than tens of meters achieved with the proposed Lorentz-force only controller. In fact, a Lorentz-force only controller can be designed using the Lorentz force/impulsive thrust controller from [13] for the full differential element state. The continuous and impulsive control inputs from [13] are given by the LQR-like laws

$$u(t) = -R^{-1}\boldsymbol{B}^T(t)\boldsymbol{P}(t)\boldsymbol{x}(t), \qquad t \neq t_k \tag{22}$$

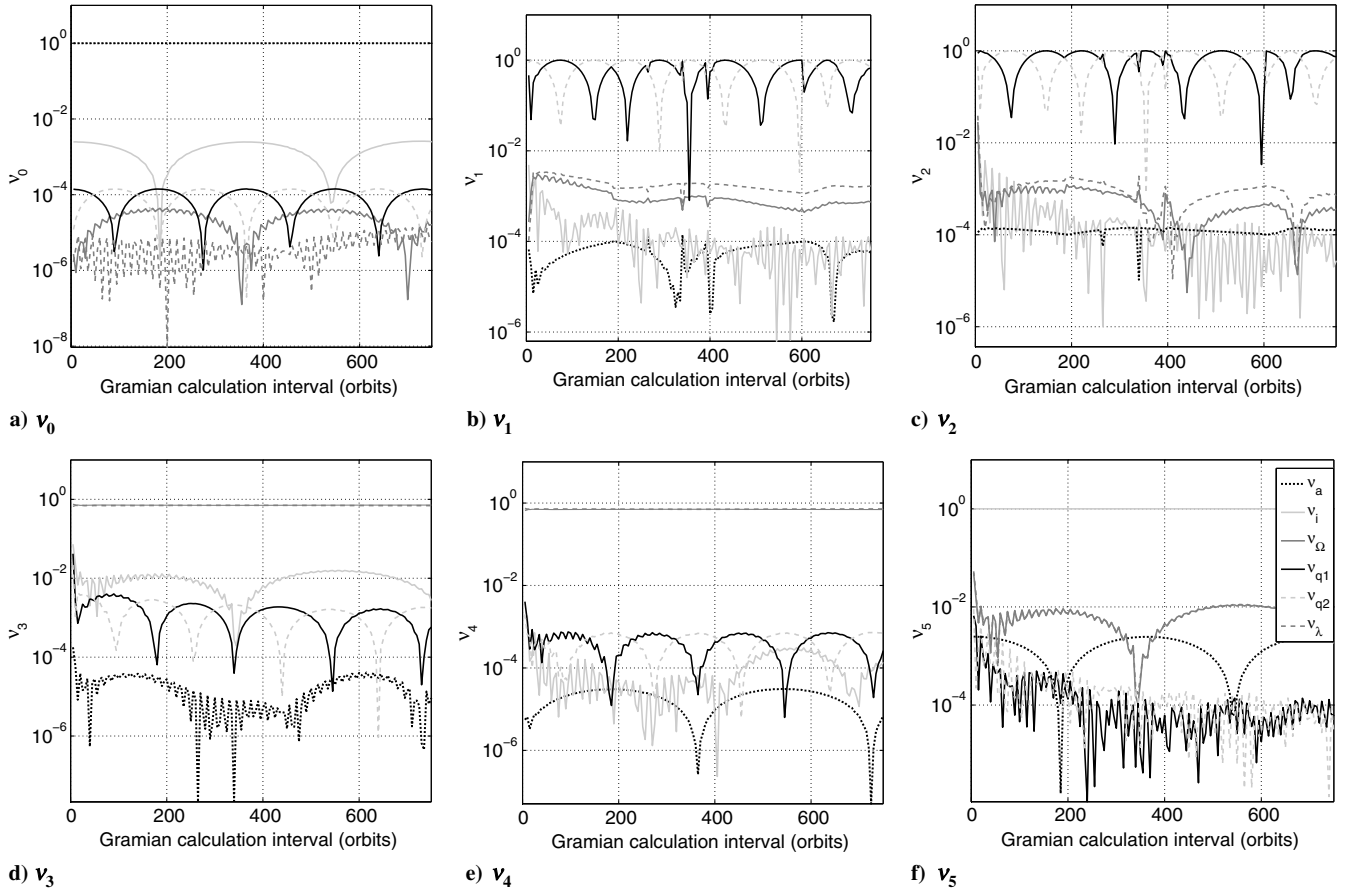

Fig. 4 Component magnitudes of the eigenvectors ν_0–ν_5 of the controllability Gramian for the Lorentz-augmented differential element system, for an equatorial, LEO.

$$\boldsymbol{v}_k = -\boldsymbol{R}_k^{-1}\boldsymbol{B}_k^T(t_k)[\boldsymbol{P}(t_k^-) - \boldsymbol{Q}_k]\boldsymbol{x}(t_k^-), \qquad t = t_k \tag{23}$$

where $\boldsymbol{v}_k$ is the impulsive thrust, t_k is the impulse application time, and $t_k{}^-$ is the time immediately before the impulse is applied.

If the impulsive control penalty, $\boldsymbol{R}_k$, is chosen to be sufficiently large, the resulting impulsive control commands an impulsive control that is sufficiently small to be neglected entirely. The polar orbit 1 km formation is considered again and continuous/impulsive control strategies are designed for three different impulsive control penalties: $\boldsymbol{R}_k = 10^6 \cdot \mathbf{1}$, $\boldsymbol{R}_k = 10^8 \cdot \mathbf{1}$, and $\boldsymbol{R}_k = 10^{10} \cdot \mathbf{1}$. The control laws use four impulsive thrusters per orbit, spaced equally over the orbit. The relative positive error norms for the three penalty cases are plotted in Fig. 7. The case $\boldsymbol{R}_k = 10^6 \cdot \mathbf{1}$ requires a modest, but significant, amount of thruster ΔV of 1.3 mm/s per orbit and achieves a relative position error norm with a maximum amplitude of less than 5 m. The increased impulsive input penalties in the two cases results in a per orbit total required thruster ΔV s of 0.25 mm/s per orbit and 4.6×10^{-3} mm/s per orbit, for the 10^8 and 10^{10} cases, respectively. For the latter case in particular, the applied thruster ΔV is insignificant. The position error norm shown in Fig. 7 for the 10^{10} case was achieved without applying the negligible thruster ΔV, again demonstrating Lorentz-force only formation maintenance. Note the resulting position error norm for the 10^{10} case is comparable to those obtained with the asymptotic LQR. Lastly, we point out that a typical charge/discharge time in LEO is 1.4 s. This value limits the bandwidth of the control but not at the time scale of interest here.

The closed-loop system using the asymptotic LQR is periodic with synodic period of the spacecraft with respective to the geomagnetic field, so Floquet analysis is used to validate the system's closed-loop stability. The closed-looped Kalman decomposed model is

$$\dot{\hat{\boldsymbol{x}}}(t) = \begin{bmatrix} \hat{\boldsymbol{A}}_c - R^{-1}\hat{\boldsymbol{B}}_c(t)\hat{\boldsymbol{B}}_c^T(t)\boldsymbol{P}_{\text{ss}} & \hat{\boldsymbol{A}}_{\text{cu}} \\ 0 & \hat{\boldsymbol{A}}_u \end{bmatrix}\hat{\boldsymbol{x}}(t) \tag{24}$$

Per Floquet theory, a periodic, time-varying system is stable if the system's state transition matrix calculated for one period of the system has eigenvalues whose magnitudes are less than unity.

Table 2 presents the eigenvalues of the state transition matrices corresponding to the closed-loop Lorentz-augmented systems for the discussed polar and equatorial cases. For both cases, there are five eigenvalues with magnitudes less than unity. The sixth eigenvalue is of unity magnitude, indicating that its mode is periodic. Examination of the eigenvectors of the closed-loop state transition reveals that the unity eigenvalue belongs to the uncontrolled mode of the decomposed system. We conclude that, as expected, the asymptotic LQR stabilizes the controllable subsystem, whereas the uncontrollable subspace remains stable in the sense of Lyapunov, which agrees with our earlier analysis of the open-loop system.

Table 1 Chief and deputy spacecraft initial conditions

	$\bar{a}$ [m]	$\bar{i}$[deg]	$\bar{\Omega}$[deg]	$\bar{q}_1$[−]	$\bar{q}_2$[−]	$\bar{\lambda}$[deg]
			Chief mean elements			
	6892000	— —	0.0	0.001	0.0	0.0
Case			Deputy mean differential elements			
$\bar{i}_c \approx 0$ deg	−0.1129	8.313×10^{-3}	-2.659×10^{-8}	7.746×10^{-9}	-7.255×10^{-5}	-2.019×10^{-6}
$\bar{i}_c = 90$ deg	1.484×10^{-4}	8.313×10^{-3}	-1.122×10^{-9}	-1.461×10^{-9}	-7.255×10^{-5}	-2.072×10^{-6}

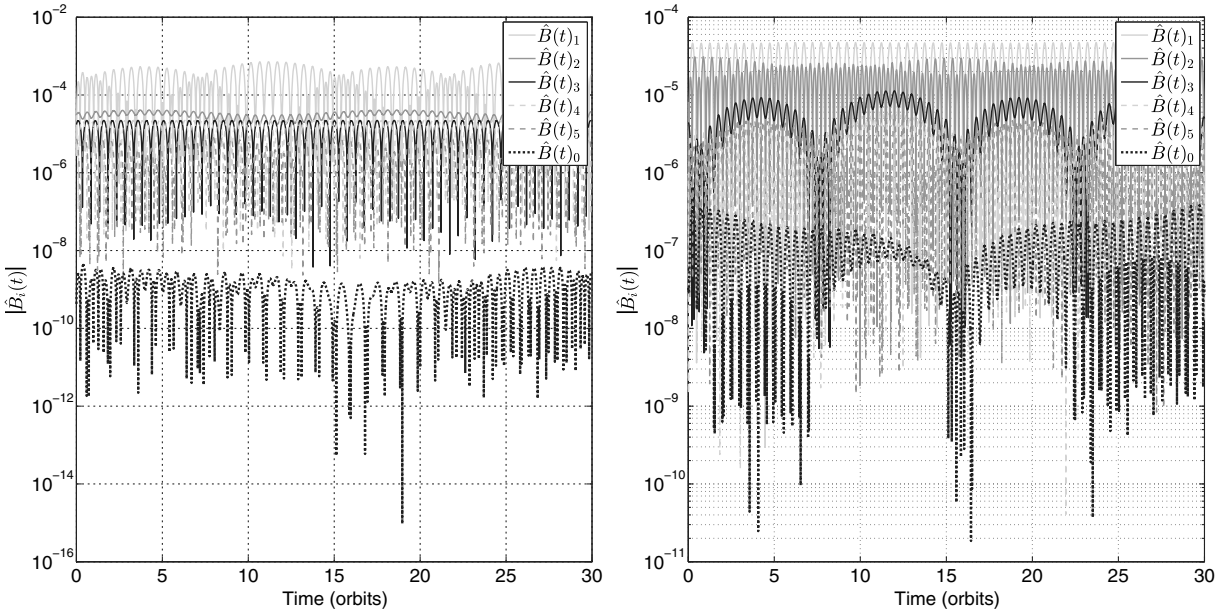

a) Equatorial reference orbit **b) Polar reference orbit**

Fig. 5 Component magnitudes of the transformed input matrix, $B(t)$, for equatorial and polar reference orbits.

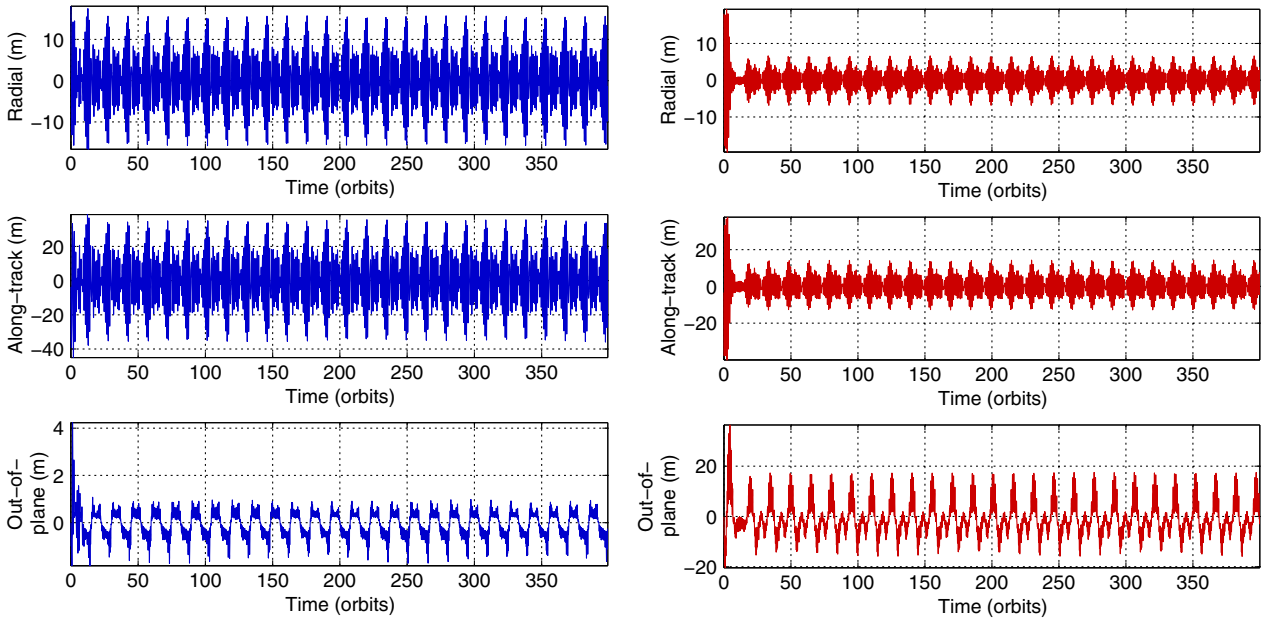

a) Equatorial reference orbit **b) Polar reference orbit**

Fig. 6 Relative position formation-keeping errors for a 1 km PCO formation in equatorial and polar LEO.

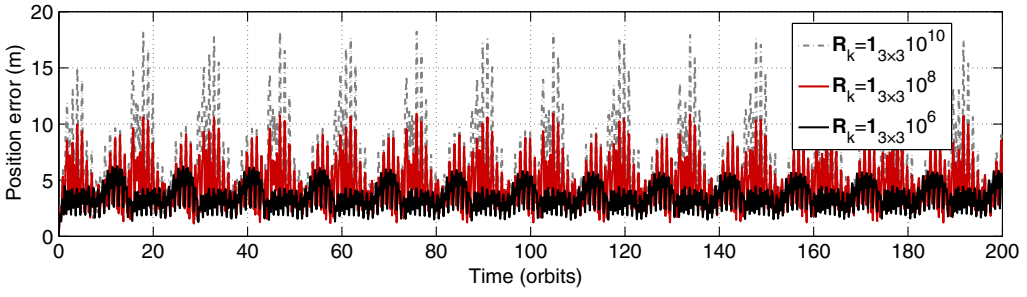

Fig. 7 Relative position error norms achieved with a combined Lorentz force/impulsive thruster controller for different impulsive control penalties, R_k.

Table 2 Eigenvalues of the state transition matrix of the closed-loop Lorentz-augmented system

Case	$\lvert\lambda_1\rvert$	$\lvert\lambda_2\rvert$	$\lvert\lambda_3\rvert$	$\lvert\lambda_4\rvert$	$\lvert\lambda_5\rvert$	$\lvert\lambda_6\rvert$
$\bar{i}_c \approx 0$ deg	1.5284×10^{-17}	5.0672×10^{-2}	5.0672×10^{-2}	0.1150	0.1150	1.00000
$\bar{i}_c = 90$ deg	4.5473×10^{-18}	3.7344×10^{-9}	6.0324×10^{-5}	1.9112×10^{-4}	3.2301×10^{-2}	0.99994

VI. Conclusions

Spacecraft formation keeping in the presence of the J_2 perturbation has been demonstrated using only the Lorentz force, i.e., with no additional thruster actuation to render the relative dynamics fully controllable. Kalman decomposition has been used to isolate the controllable subspace of the dynamics for controller design, where its application to a time-varying system has been justified by demonstrating that the uncontrollable subspace of the system is time-invariant. Floquet analysis shows that the eigenvalue of the uncontrollable mode for a Lorentz-augmented formation in polar and the equatorial orbit lies on the unit disc. For those two cases, any state error in the uncontrollable mode will result in a nonzero but bounded relative position error. For formations in other inclinations, a similar analysis is required.

Although not demonstrated in this Note, the presented results indicate that it should be possible to perform formation maneuvers beyond just perturbation mitigation using only the Lorentz force, provided that the target state does not require a change to the uncontrollable state. For example, in equatorial orbits, where the uncontrollable state is equal to the differential semimajor axis, the $\delta\bar{a}$ of the target formation state must be equal to the $\delta\bar{a}$ of the current formation state. Conversely, if there are situations where the uncontrollable state must be altered, Lorentz-augmented spacecraft will still require propellant for conventional thruster actuation.

References

[1] Saaj, C., Lappas, V., Richie, D., Peck, M., Streetman, B., and Schaub, H., "Electrostatic Forces for Satellite Navigation and Reconfiguration," European Space Agency, Ariadna Final Rept. 05-4107b, 2006.

[2] Peck, M., "Prospects and Challenges for Lorentz-Augmented Orbits," *AIAA Guidance, Navigation, and Control Conference and Exhibit*, AIAA Paper 2005-5995, 2005. doi:10.2514/6.2005-5995

[3] Streetman, B., and Peck, M., "General Bang-Bang Control Method for Lorentz Augmented Orbits," *Journal of Spacecraft and Rockets*, Vol. 47, No. 3, 2010, pp. 484–492. doi:10.2514/1.45704

[4] Atchison, J., and Peck, M., "Lorentz-Augmented Jovian Orbit Insertion," *Journal of Guidance, Control, and Dynamics*, Vol. 32, No. 2, 2009, pp. 418–425. doi:10.2514/1.38406

[5] Streetman, B., and Peck, M., "Gravity-Assist Maneuvers Augmented by the Lorentz Force," *Journal of Guidance, Control, and Dynamics*, Vol. 32, No. 5, 2009, pp. 1639–1647. doi:10.2514/1.35676

[6] Peck, M. A., Streetman, B., Saaj, C. M., and Lappas, V., "Spacecraft Formation Flying Using Lorentz Forces," *Journal of British Interplanetary Society*, Vol. 60, No. 7, 2007, pp. 263–267.

[7] Yamakawa, H., Bando, M., Yano, K., and Tsujii, S., "Spacecraft Relative Dynamics Under the Influence of the Geomagnetic Lorentz Force," *AIAA Guidance, Navigation, and Control Conference*, AIAA Paper 2010-8128, 2010. doi:10.2514/6.2010-8128

[8] Tsujii, S., Bando, M., and Yamakawa, H., "Spacecraft Formation Flying Dynamics and Control Using the Geomagnetic Lorentz Force," *Journal of Guidance, Control, and Dynamics*, Vol. 36, No. 1, 2013, pp. 136–148. doi:10.2514/1.57060

[9] Pollock, G. E., Gangestad, J., and Longuski, J., "Analytical Solutions for the Relative Motion of Spacecraft Subject to Lorentz-Force Perturbations," *Acta Astronautica*, Vol. 68, No. 1, 2011, pp. 204–217. doi:10.1016/j.actaastro.2010.07.007

[10] Gangestad, J., Pollock, G. E., and Longuski, J., "Lagrange's Planetary Equations for the Motion of Electrostatically Charged Spacecraft," *Celestial Mechanics and Dynamical Astronomy*, Vol. 108, No. 2, 2010, pp. 125–145. doi:10.1007/s10569-010-9297-z

[11] Streetman, B., and Peck, M., "New Synchronous Orbits Using the Geomagnetic Lorentz Force," *Journal of Guidance, Control, and Dynamics*, Vol. 30, No. 6, 2007, pp. 1677–1689. doi:10.2514/1.29080

[12] Sobiesiak, L., and Damaren, C., "Hybrid Periodic Differential Element Control Using the Geomagnetic Lorentz Force," *AIAA/AAS Astrodynamics Specialist Conference*, AIAA Paper 2012-4584, 2012. doi:10.2514/6.2012-4584

[13] Sobiesiak, L. A., and Damaren, C. J., "Optimal Continuous/Impulsive Control for Lorentz-Augmented Spacecraft Formations," *Journal of Guidance, Control, and Dynamics*, Vol. 38, No. 1, 2015, pp. 151–156. doi:10.2514/1.G000334

[14] Brouwer, D., "Solutions of the Problem of Artificial Satellite Theory Without Drag," *Astronomical Journal*, Vol. 64, No. 1274, 1959, pp. 378–396. doi:10.2514/1.57060

[15] Gim, D., and Alfriend, K., "State Transition Matrix of Relative Motion for the Perturbed Noncircular Reference Orbit," *Journal of Guidance, Control, and Dynamics*, Vol. 26, Nov.–Dec. 2003, pp. 956–971. doi:10.2514/2.6924

[16] Schaub, H., and Junkins, J. L., *Analytical Mechanics of Space Systems*, AIAA Education Series, AIAA, Reston, VA, 2003, pp. 533, 573–576.

[17] Breger, L., and How, J. P., "Gauss's Variational Equation-Based Dynamics and Control for Formation Flying Spacecraft," *Journal of Guidance, Control, and Dynamics*, Vol. 30, No. 2, 2007, pp. 437–448. doi:10.2514/1.22649

[18] Streetman, B., "Lorentz-Augmented Orbit Dynamics and Mission Design," Ph.D. Dissertation, Cornell Univ., Ithaca, NY, 2008.

[19] Psiaki, M. L., "Magnetic Torquer Attitude Control via Asymptotic Periodic Linear Quadratic Regulation," *Journal of Guidance, Control, and Dynamics*, Vol. 24, No. 2, 2001, pp. 386–394. doi:10.2514/2.4723

[20] Wertz, J. R., *Spacecraft Attitude Determination and Control*, Reidel Publ. Company, Dordrecht, The Netherlands, 1978, pp. 782–784.